Annu. Rev. Biophys. Biomol. Struct. 2004. 33:245–68
doi: 10.1146/annurev.biophys.33.110502.132716

First published online as a Review in Advance on January 16, 2004

ROTATION OF F_1-ATPASE: How an ATP-Driven Molecular Machine May Work

Kazuhiko Kinosita, Jr.,[1] Kengo Adachi,[1] and Hiroyasu Itoh[2,3]
[1]*Center for Integrative Bioscience, Okazaki National Research Institutes, Higashiyama 5-1, Myodaiji, Okazaki 444-8585, Japan; email: kazuhiko@ims.ac.jp; adachi@ims.ac.jp*
[2]*Tsukuba Research Laboratory, Hamamatsu Photonics KK, and* [3]*CREST "Creation and Application of Soft Nano-Machine, the Hyperfunctional Molecular Machine" Team 13*, Tokodai, Tsukuba 300-2635, Japan; email: hiritoh@hpk.trc-net.co.jp*

Key Words molecular motor, single-molecule physiology, torque generation, efficiency of energy conversion, free energy

■ **Abstract** F_1-ATPase is a rotary motor made of a single protein molecule. Its rotation is driven by free energy obtained by ATP hydrolysis. In vivo, another motor, F_o, presumably rotates the F_1 motor in the reverse direction, reversing also the chemical reaction in F_1 to let it synthesize ATP. Here we attempt to answer two related questions, How is free energy obtained by ATP hydrolysis converted to the mechanical work of rotation, and how is mechanical work done on F_1 converted to free energy to produce ATP? After summarizing single-molecule observations of F_1 rotation, we introduce a toy model and discuss its free-energy diagrams to possibly answer the above questions. We also discuss the efficiency of molecular motors in general.

CONTENTS

1056-8700/04/0609-0245$14.00

INTRODUCTION

F_1-ATPase

F_1-ATPase is a part of the enzyme ATP synthase that synthesizes ATP from ADP and inorganic phosphate (Pi) using proton flow across the membrane as the energy source (10, 26, 60, 67). The membrane-embedded F_o portion conducts protons, which drive the catalytic synthesis of ATP in the water-soluble F_1 portion. The ATP synthase is a reversible molecular machine in that hydrolysis of ATP in F_1 can pump protons through F_o in the opposite direction against an electrochemical gradient of protons. To explain the energetic coupling between the proton flow in F_o and synthesis/hydrolysis of ATP in F_1, Boyer & Kohlbrenner (12) and Oosawa and colleagues (17, 43) independently proposed rotational catalysis at about the same time, although a full account of the latter's model (44) appeared late. The prediction was that both F_o and F_1 are rotary motors, F_o being powered by proton flow and F_1 by ATP hydrolysis, and that the genuine rotary directions of the two are opposite to each other yet the two have a common rotary shaft (rotor). When the drop of proton electrochemical potential across the membrane exceeds the free energy obtained by ATP hydrolysis, F_o wins and F_1 is forced to rotate in its reverse direction, resulting in the synthesis of ATP in its catalytic sites. If the free energy of ATP hydrolysis is larger, rotation is in the direction of F_1 and protons are pumped back. Crystal structures of F_1 (1) and F_oF_1 (53) suggested that the two are indeed rotary motors, and unidirectional rotation, counterclockwise when viewed from the F_o side, was videotaped for an isolated F_1 attached to a glass surface (40). For the whole ATP synthase, reorientation of γ under proton-motive force has been indicated in a cross-linking study (68), and single-molecule study (9a) has suggested rotation. Proton driven rotation, clockwise and stepwise, has recently been demonstrated in a fluorescence resonance energy transfer study (70).

Isolated F_1, consisting of $\alpha_3\beta_3\gamma\delta\varepsilon$ subunits (in bacteria), only hydrolyzes ATP and hence is called F_1-ATPase. An $\alpha_3\beta_3\gamma$ subcomplex suffices for rotation and hydrolysis activities: The central γ subunit rotates inside a cylinder made of three α and three β subunits arranged alternately (Figures 1 and 2) when ATP is hydrolyzed in three catalytic sites each hosted primarily by a β subunit. In this article, we focus on this simplest subcomplex and, hereafter, refer to it simply as F_1.

The Question

The central question we ask in this article is, How are the chemical reactions, synthesis or hydrolysis of ATP, in the catalytic sites coupled to the mechanical

rotation of γ? Hydrolysis of one molecule of ATP accompanies a free-energy drop ΔG of

$$\Delta G = \Delta G_0 + k_B T \ln[\mathrm{ADP}][\mathrm{Pi}]/[\mathrm{ATP}], \quad 1.$$

where $\Delta G_0 = -50$ pN · nm is the standard free-energy change at pH 7 (6; also see recent beautiful work in Reference 56), and $k_B T = 4.1$ pN · nm is the thermal energy at room temperature (k_B, the Boltzmann constant; T, absolute temperature). Under physiological conditions of [ATP] $\sim 10^{-3}$ M, [ADP] $\sim 10^{-4}$ M, and [Pi] $\sim 10^{-3}$ M, ΔG is about -90 pN · nm. ΔG is negative under all practical conditions, implying that the reaction always proceeds in the direction of hydrolysis and that spontaneous net synthesis of ATP never happens in solution. How, then, is this chemical reaction, which is destined to proceed in one direction, converted to unidirectional rotation that can do work against an external opposing torque?

In this article, we first summarize rotational characteristics of F_1 revealed by single-molecule observations. The results allow us to deduce potential energies for γ rotation in various chemical states. We then try to answer the central question on the basis of these potential energies. In doing so, we introduce a toy model that can reproduce the experimental potential energies and that, if fabricated by future nanotechnology, would work as an ATP-driven rotary motor. Our goal is to show a possible, concrete mechanism of chemo-mechanical energy transduction that bears some essential features of the actual F_1 motor. We discuss how a motor senses free energy of ATP hydrolysis and how it responds to an external load. Our discussion is yet premature and may contain incorrect statements, but we hope that some of the concepts we present here may be useful in interpreting or designing future experiments.

ROTATION OF F_1

Single-Molecule Observations of F_1 Rotation

Counterclockwise rotation was first imaged in F_1 from a thermophilic bacterium by attaching a fluorescent actin filament to γ while fixing the $\alpha_3\beta_3$ cylinder to a glass surface (40). Since then, counterclockwise rotation has been confirmed in F_1 from *Escherichia coli* (39, 41) and plants (19). Rotation of tags other than actin has been imaged successfully (2), including a single fluorophore (2a), spherical bead or bead duplex (18, 65), metal bar (52), or a single donor-acceptor pair for fluorescence resonance energy transfer (9, 63). Subunits attached to γ rotate counterclockwise during ATP hydrolysis, suggesting that they are part of the common rotor shaft in the whole ATP synthase: the ε subunit (24) and the ring of c subunits in F_o (37, 49, 55), but not the a subunit of F_o (37), which is considered to be part of the stator. V_1-ATPase, a relative of F_1-ATPase, also rotates in the same direction (21).

Below we summarize the rotational characteristics of the F_1 motor that are essential to the understanding of the mechanism of chemo-mechanical coupling.

Most of the quoted results were obtained with F_1 from a thermophilic bacterium (40). Details of earlier work have been reviewed elsewhere (26, 67).

120° STEP PER ATP For ATP concentrations, [ATP], from 20 nM to 6 mM, rotation occurs in discrete 120° steps (2a, 64, 65). The time-averaged stepping rate depends on [ATP] in a Michaelis-Menten manner, with a V_{max} of 390 steps s^{-1} and K_m of 15 μM (65). Statistical analysis of intervals between steps at various [ATP] indicates that each step is driven by the hydrolysis of one ATP molecule (2a, 64, 65). The average stepping rate of single molecules above, however, is somewhat higher than the hydrolysis rate measured in solution (65), apparently suggesting that the coupling ratio, the number of 120° steps per ATP molecules consumed, is greater than 1. Presumably, the hydrolysis rate is underestimated, because part of F_1 in solution is inhibited by MgADP (10, 18, 23, 26, 32), whereas a single-molecule observation focuses on active molecules in the field of view (26). Our expectation is that the coupling ratio is close to but slightly less than 1.

ANGLE-INDEPENDENT TORQUE When a micrometer-sized actin filament is attached to γ, F_1 rotates slowly because of the hydrodynamic friction against the moving actin filament. The frictional drag coefficient, ξ, is given (2, 20) by:

$$\xi = (4\pi/3)\eta L^3/[\ln(L/r) - 0.447] \qquad 2.$$

for an actin filament of length L and radius r ($\sim$5 nm) rotating around one end, where η is the viscosity of the medium and is $\sim 10^{-3}$ Nm^{-2} s at room temperature. (This equation was mistyped in some of our earlier work.) If, instead of actin, a spherical bead of radius a is attached off axis such that the distance between the bead center and rotation axis is x, ξ is given by:

$$\xi = 8\pi\eta a^3 + 6\pi\eta a x^2. \qquad 3.$$

The torque N needed to rotate the filament against the friction is given by:

$$N = \omega\xi, \qquad 4.$$

where ω is the speed of rotation (in radians s^{-1}). From the rotation speed during each 120° step, the torque F_1 produces against the friction is estimated to be $\sim$44 pN · nm; the torque appears independent of the rotary angle, because the rotation speed is constant during a 120° step (25). A similar value of 40 pN · nm is obtained from the rotation speed averaged over many revolutions, under the condition of high enough [ATP] in which F_1 bearing an actin filament rotates smoothly without apparent steps (64). Thus, the work F_1 can do in a 120° step amounts to 80–90 pN · nm or $\sim$20 k_BT, calculated as 40–44 pN · nm × $(2/3)\pi$ radian (=120°). This is almost equal to the physiological $|\Delta G|$ for ATP hydrolysis above, suggesting that the energy conversion efficiency, the average work done in a 120° step divided by $|\Delta G|$, can reach $\sim$100% (but see below). The torque of $\sim$44 pN · nm may be somewhat underestimated, because the friction near a glass surface

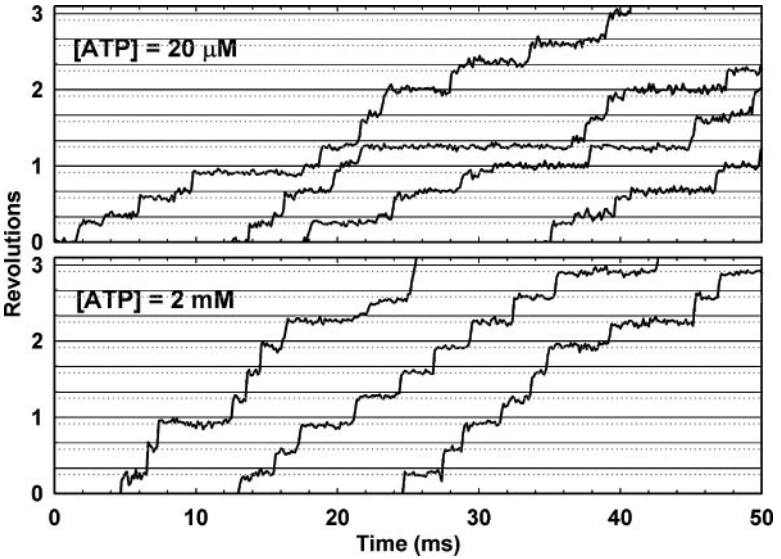

Figure 3 Substeps in F_1 rotation at 20 μM ATP (*upper panel*) recorded with a temporal resolution of 0.125 ms (65). With this resolution, substeps are not discerned at 2 mM ATP (*lower panel*), implying that the ATP-waiting dwell is <0.125 ms and the next 90° rotation is complete within 0.125 ms of ATP binding; it also implies that F_1 is completely reset and ready to bind a next ATP by the end of a 30° substep. Horizontal solid lines are separated by 120°, and dotted lines are drawn 30° below.

is higher than the estimate in Equations 2 and 3 (20). A slightly higher value, 50 pN · nm, has been estimated from the curvature of an actin filament attached to γ (45). Here, the torque of F_1 is balanced by the elastic recoil of a bent actin, which, unlike friction, is a conservative force.

80°–90° SUBSTEP BY ATP BINDING AND 40°–30° SUBSTEP BY PRODUCT RELEASE A 40-nm gold bead attached to γ (Figure 1) does not impede rotation, at least as far as the average stepping rate is concerned, even though the bead is approximately four times as large as F_1. Figure 3 shows time courses of the bead rotation recorded at 8000 frames s^{-1} (65). At 20 μM ATP, the 120° steps are resolved into ~90° and ~30° substeps, as seen in most parts of the record. The dwell before a 90° substep is much longer, on average, at lower [ATP], and the average dwell is inversely proportional to [ATP]. This implies that the 90° substep is triggered by binding of ATP. Because the 90° rotation is complete within 0.125 ms of ATP binding (Figure 3, *lower panel*), most of the 90° rotation seems to be driven directly by ATP binding, and not by a subsequent process such as ATP hydrolysis.

The dwell time before a 30° substep is independent of [ATP]. Analysis indicates that the dwell consists of at least two reactions, each taking ~1 ms (65). Because a

30° substep is immediately (<0.125 ms) followed by a 90° substep at 2 mM ATP (Figure 3, *lower panel*), the 30° substep completely resets the motor to the initial ATP-waiting state. The simplest scenario is that the 30° substep is driven by the release of a hydrolysis product, ADP or Pi, whichever is released last.

When F_1 falls into the MgADP-inhibited state and stops rotating, it stalls at the ∼80° position (18). This is consistent with the idea that the 30° substep is associated with ADP release, of which the failure leads to inhibition. Or, the 30° substep may be driven by Pi release, which induces a conformational change in F_1 (31). When rotation is driven by ATP-γ-S, which is slowly hydrolyzed by F_1, video-rate substeps of ∼80° and ∼40° are observed (50), indicating that ATP hydrolysis occurs before the 30° substep and supporting the contention that ATP binding drives most (80°) of the 90° substep. A fluorescent ATP analog (Cy3-ATP) also induces video-rate substeps of ∼80° and ∼40° in a mutant F_1, and binding/release of Cy3-ATP has been imaged simultaneously with the substep rotation (37a). This study, combined with the ATP-γ-S study above (50), indicates that one of the two ∼1 ms reactions preceding the 30° substep is the ATP hydrolysis in a site that bound ATP one step ago. These more recent results suggest that 80° rather than 90° is closer to the actual substep size, the difference being an experimental error, or that the 80° rotation is driven by ATP binding and the remaining 10° by another process such as ATP hydrolysis.

Potential Energy for γ Rotation

The scheme that emerges from these studies for the potential energy of γ rotation is shown in Figure 4. We distinguish at least three states (A)-(C), (A) being the ATP-waiting state and (A′) being the next ATP-waiting state. For the chemical species involved in rotation, two basic schemes have been proposed: a bi-site scheme in which the occupancy of catalytic sites alternates between 1 and 2 (Figure 4*b*), and a tri-site scheme alternating between 2 and 3 (Figure 4*c*). Previously, we suggested that the bi-site scheme would be the norm because earlier studies (35) indicated bi-site operation at least at low [ATP] and because the rotation rate is characterized by a single K_m down to 20 nM ATP (65). Site occupancy probed by a tryptophan residue engineered in the catalytic sites, however, is more than 2 at ≥10 μM ATP, and steady-state hydrolysis activity correlates well with the fraction of molecules with an occupancy number of ≥2 (42, 47, 59). Weber & Senior (59, 60) thus conclude that three-site filling is a must for rotation. A crystal structure in which three sites are occupied with a nucleotide (34) also supports a tri-site scheme. Work in our lab is as yet inconclusive: Rotation driven by Cy3-ATP proceeds in a tri-site mode (37a), whereas analysis of fluorescence resonance energy transfer apparently suggests bi-site if crystal structures of mitochondrial F_1 are undistorted by crystal packing (63). The average stepping rate is proportional to [ATP] down to 0.6 nM ATP (N. Sakaki, unpublished results), suggesting that, if it operates in a tri-site mode, two catalytic sites bind a nucleotide extremely tightly, apparently in contradiction to the binding data above. Boyer (11) suggests that bi-site is fundamental, but retention of the ADP to be released may lead to three-site filling.

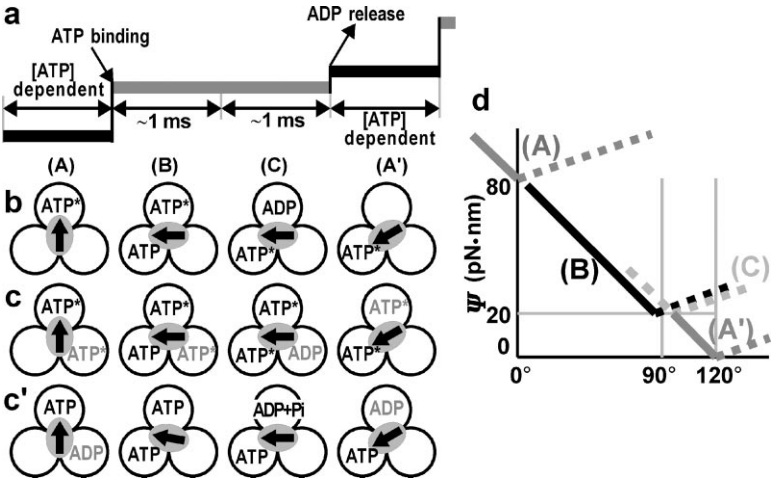

Figure 4 Potential energy for γ rotation deduced from the substep behavior (65). (*a*) Schematic diagram of 90° and 30° substeps. (*b*) Corresponding nucleotide states in a bi-site scheme. The central arrow shows the orientation of γ. ATP* represents ATP or ADP + Pi; ADP may be ADP + Pi or Pi. (*c*) A tri-site scheme. Light shade indicates difference in site occupancy. (*c′*) A tri-site scheme that is closer to *b* is also possible, in which site occupancy remains 2 and becomes 3 only during the 90° substep. (*d*) Potential energies for the four chemical states (A)-(A′). The γ orientation in state (A) is taken as 0°. The vertical shifts of the potential curves in this figure are arbitrary. See Figures 7 and 8 and associated explanations in text.

ATP binding may indeed assist release of a retained ADP (K. Adachi, unpublished data) (Figure 4*c′*). More work is needed before concluding firmly that three sites must be filled for rotation to occur. In this article, we define states (A) and (A′) in Figure 4 as the ATP-waiting state, and (B) as the state immediately after ATP binding, regardless of the actual occupancy number.

The scheme in Figure 4*a* and the angle-independent torque of 40–44 pN · nm suggest a potential energy diagram for γ rotation in each chemical state, as in Figure 4*d*. Here, solid lines reflect the experimental constant torque, and dashed lines are added to provide minima at the experimentally observed stationary angles. In the ATP-waiting state (A), γ rests at the potential minimum at 0°. Binding of ATP changes the state to (B), whereupon γ slides down the constant slope toward the minimum at 90°. The chemical transition from (B) to (C) is mechanically almost silent. Release of the last hydrolysis product restores state (A′), whereupon γ slides down the slope for the last 30°. As noted above, the minima for (B) and (C) may well be closer to 80°, or the minimum for (B) near 80° and that for (C) near 90°.

F_1 rotation can be driven by GTP and ITP, but not by CTP and UTP at concentrations up to 300 μM (38). The Michaelis-Menten constant, K_m, for hydrolysis

differs among ATP, GTP, and ITP, but all these purine nucleotides drive an actin filament at similar speeds, implying similar torque. Thus, it appears that the potential energies in Figure 4*d* are the properties intrinsic to F_1, and nucleotides are either able or unable to drive transitions among the potential curves.

How an ATP-Driven Molecular Machine May Work

The potential diagram in Figure 4*d* is our experimental answer to the prime question of how a molecular machine can convert free energy of ATP hydrolysis into work. We believe that protein machines work by changing their conformations. In the case of F_1, rotation of γ is in itself a sequence of conformational changes of F_1, and individual β subunits, in particular, undergo large conformational changes in response to nucleotide binding (Figure 2). Each potential curve in Figure 4*d* thus represents the change in conformational energy of the protein (F_1) in that chemical state, as γ is rotated to designated angles. Before discussing how these potentials could explain rotation, let us summarize in Figure 5 what the experiments have told us. A protein molecule, shown in green, is to do mechanical work by changing its conformation between the upright posture and bent one.

MAJOR WORK IS DONE BY ATP BINDING, AND SOME BY PRODUCT RELEASE At least in F_1, the major, work-producing conformational change (80°–90° rotation) is driven by ATP binding. Another change, back to the original conformation upon product release, also does some positive work. ATP hydrolysis per se does not contribute much to work output. In other words, major free-energy drops, which can be converted to work, occur upon ATP binding and product release (brown arrows in Figure 5). Indeed, on a protein machine such as F_1 and myosin, ATP and its hydrolysis products ADP + Pi are near equilibrium, as demonstrated by spontaneous ATP synthesis on these proteins in the presence of high concentrations of ADP and Pi (30, 48, 61, 66). Exploiting binding and release, rather than hydrolysis, seems natural if one is to design an efficient protein machine: Upon substrate binding, many bonds are newly formed between the substrate and protein, whereas hydrolysis would result mainly in bond reorganization without a gross change in the total number of bonds.

NUCLEOTIDE AFFINITY CHANGES AS ROTATION (CONFORMATIONAL CHANGE) PROCEEDS If ATP binding drives a conformational change in a protein molecule, that particular conformational change will accompany an increase in the affinity for ATP, by the law of action and reaction. Likewise, if ADP (Pi) release drives another conformational change, that will accompany a decrease in the affinity for ADP (Pi). These points are crucial in understanding the mechanism of the F_1 motor and molecular machines in general.

A highly schematic explanation is given in Figure 5 for the case of ATP binding. Starting from the upper left, initial binding of ATP (light color) is accomplished by the formation of multiple weak bonds (violet dots). The fact that ATP binding

induces bending (conformational change) of the protein implies that the ATP molecule pulls the protein toward it by forming more bonds (second from left). As a result, the ATP molecule in the bent protein is now tightly held in the bent protein, implying higher affinity. Constant torque can be explained by sequential increase in the number of bonds. A more realistic view for the particular case of F_1 has been given by molecular dynamics simulation (3).

The magnitude of affinity changes can be estimated by referring to Figure 4*d* (65). As γ is rotated from 0° to 90°, curve (B) for the ATP-bound state becomes lower (more stable) than curve (A) for the state before ATP binding. The stabilization upon the 90° rotation amounts to >60 pN · nm in energy, or to an increase in the affinity for ATP of more than $\exp(60\ \text{pN} \cdot \text{nm}/k_BT) \sim 2 \times 10^6$-fold. Similarly, rotation from 90° to 120° is accompanied by a decrease in the affinity for ADP (Pi) of more than $\exp(20\ \text{pN} \cdot \text{nm}/k_BT) \sim$100-fold.

THE PRIMARY ROLE OF HYDROLYSIS IS TO RESET THE MACHINE If work is done by binding and release, why is ATP hydrolyzed? The reason is that, after the ATP-driven conformational change, the ATP molecule is so tightly bound that the reaction stops there (second from left in Figure 5). To remove this blocking ATP, the protein machine splits it into two entities so that individual products, each held by a smaller number of bonds, can escape one by one.

In the case of F_1, which synthesizes ATP efficiently upon reverse rotation, we propose (25, 26) that hydrolysis may well produce some work (rotation), although direct evidence is not yet available. The model below considers this possibility.

A CAMSHAFT MODEL OF F_1 ROTATION

Here we present a simple mechanical model (Figure 6) that is based on the models of Oosawa & Hayashi (44) and of Wang & Oster (57). The purpose is to show a relatively concrete example of the mechanism of chemo-mechanical energy conversion that mimics some of the essential features of the F_1 motor. For the purpose of illustration, we design the model to work in a bi-site scheme at moderate ATP concentrations, because a smaller number of chemical pathways need to be considered in bi-site. Most of the discussion below, however, is independent of the details of chemical pathways and thus is applicable to a tri-site scheme as well.

A Push-Pull Mechanism for Torque Generation

As seen in Figure 2, crystal structures of mitochondrial F_1 (1, 15) have shown that a β subunit binding a nucleotide is bent in such a way that its upper portion pushes γ toward and beyond the central axis. An empty β, on the other hand, retracts and pulls γ toward it; an isolated β subunit (62) or βs in an $\alpha_3\beta_3$ complex without γ (51) adopt a conformation similar to the empty β in the whole F_1,

although a recent simulation shows otherwise (8). Wang & Oster (57) have proposed that these push-pull actions against the slightly slant and skewed γ constitute the driving force of rotation. This is consistent with the fact that, in the upper and lower portions of the central cavity of the $\alpha_3\beta_3$ cylinder where γ makes extensive contacts with the cylinder wall (Figure 2, *top*), the cylinder wall is covered with hydrophobic residues (1), allowing lateral slippage while responding to push and pull. The contact at the γ tip (at the lower end of and as illustrated in the top part of Figure 2) seems relatively unimportant, because up to 12 residues can be removed without affecting torque (36). Another major contact is made between γ and the top surface of a β, near the orifice. The contact area of β, the so-called DELSEED motif (yellow atoms in Figure 2, *top, left*), contains a cluster of conserved acidic residues, suggesting a role in torque generation. Complete elimination of the negative charges, however, did not affect the rotational characteristics (16), although molecular dynamics simulation suggests a role for this region (29). Thus, we also assume that the push-pull actions by β are the major source of the torque, and we model γ as a camshaft and let bending/unbending of β push/pull the camshaft (Figure 6*a*).

The push, or bending of β, is driven by ATP binding (Figure 6*b*), and conversely a bent β shows a higher affinity for ATP than an unbent β does. The pull, or unbending of β, is driven by the release of ADP (Figure 6*c*), which is assumed to dissociate last, and unbending leads to a lower affinity for ADP (and Pi). The central camshaft is so designed that ATP-driven bending of a β rotates the γ shaft by 80° (Figure 6*e*, *e*1–*e*10), and unbending of another β upon ADP release drives the last 30° from 90° to 120° (Figure 6*e*, *e*13–*e*16). By repeating the sequence in Figure 6*e*, the central γ shaft continues to make counterclockwise 120° steps (see Supplementary Movie 1; follow the Supplemental Material link from the Annual Reviews home page at http://www.annualreviews.org).

The Mechanism Warranting Unidirectional Rotation

In principle, simple pushes and pulls would rotate the shaft in either direction. In our model, there are two stages in which the γ shaft could rotate clockwise (wrong direction). The first is the situation in Figure 6*e*1, in which two βs are empty: Binding of ATP to the wrong β (β_3) would lead to clockwise rotation. Binding to the wrong β, however, is prevented by virtue of the slope of the camshaft. The radii of the cam are varied in such a way that the correct β (β_2) is already bent slightly, whereas β_3 is completely unbent. Thus, the correct β has a higher affinity for ATP, and thus, in most cases, this β binds the next ATP. In a tri-site scheme, the situation of two βs being empty does not arise. However, when ADP is to be released, one of three filled sites needs to be selected. This is equivalent to the choice of an ATP binding site, because ATP will bind to the site from which ADP has dissociated.

The next critical stage is in Figure 6*e*10, in which two βs bind ATP tightly and either ATP could be hydrolyzed. If the β that has just bound ATP (β_2) hydrolyzes

the ATP, the shaft would make a backward substep upon release of the hydrolysis products. To prevent this uncoupling scenario, we postulate (as in References 25, 26, and 44) that hydrolysis of ATP drives a small amount of counterclockwise rotation of γ (Figure 6*d*). That is, the tip of the toy β is twisted to the right (as it faces γ) when its bound ATP is split into ADP + Pi, and further as Pi is released. The law of action and reaction states, then, that twisting the tip of β to the right drives the equilibrium between ATP and ADP + Pi toward hydrolysis, and twisting to the left shifts the equilibrium toward ATP synthesis. Once we assume the coupling between the tip motion and hydrolysis/synthesis reactions, rotation in the correct direction is warranted: In Figure 6*e*10, β_1 can hydrolyze ATP by twisting its tip to the right, but β_2 cannot because the tip motion is obstructed by the cam wall. A theoretical calculation has indicated that a β that presumably has just bound ATP favors ATP over ADP + Pi (13).

Clockwise Rotation Leads to ATP Synthesis

The model predicts synthesis of ATP when the γ shaft is forcibly rotated clockwise. This can be seen by following Figure 6*e* in the reverse order (also see Supplementary Movie 2; follow the Supplemental Material link from the Annual Reviews home page at http://www.annualreviews.org). Clockwise rotation pulls in and thus bends β_1, thereby increasing its affinity for ADP (Figure 6*e*, *e*16–*e*14). Here, bending β_1 also tends to increase its affinity for ATP, but because the slope of the camshaft twists the tip of β_1 to the right, the affinity for ADP is higher. Thus, ADP and then Pi bind (Figure 6*e*, *e*13–*e*12). Further rotation twists the β_1 tip to the left (Figure 6*e*, *e*11–*e*10) to facilitate the conversion of ADP + Pi to ATP, which remains tightly bound. At this angle, the ATP that has been synthesized in the previous step is still tightly bound by β_2, but further clockwise rotation (Figure 6*e*, *e*10–*e*1) pries the catalytic site open and releases the ATP. Clockwise rotation of γ in a molecular dynamics simulation has demonstrated that the affinity for ATP decreases with rotation, as expected (7).

Recently, we have shown that ATP is indeed synthesized when the γ shaft of actual F_1 is forcibly rotated clockwise by electric magnets, through a magnetic bead attached to γ (22). An external torque applied to one point on the motor suffices to reverse the chemo-mechanical linkage and force the chemical reaction in remote catalytic sites to proceed in reverse, increasing chemical free energy. This is not a trivial result: consider whether one can pull back a linear motor, such as myosin or kinesin, to let it synthesize ATP, and, if one can, where to pull.

POTENTIAL DIAGRAMS FOR THE CAMSHAFT MODEL

Here we derive potential diagrams for the camshaft model, which basically reproduce the experimental potential diagram in Figure 4*d*, to discuss the motor's behaviors under various ΔG and under various external loads.

Free-Energy Diagrams

The three sets of curves at the bottom of Figure 7*a* show the angle-dependent energy, $\psi_i^L(\theta)$, that we assume for the interaction between γ and a β binding a ligand, L, where L is ATP (T), ADP + Pi (H), ADP (D), Pi (P), or none (E); and i = 1, 2, or 3 designates one of the three βs. These potential energies reflect the shape of the camshaft. We assume that an empty β is stable when it is unbent and that a β binding a ligand is stable when it is bent. Thus, $\psi_1^T(\theta)$, for example, is low for θ between -30° and 80°, where β_1 remains fully bent; and $\psi_1^T(\theta)$ is highest at $\theta = 100^\circ$, where β_1 with its tip twisted to the left is forced to unbend fully. $\psi_i^L(\theta)$ for L = H, D, and P have the same shape as $\psi_i^T(\theta)$, except that their heights are lower and they are shifted to the right, reflecting the twist of the β tip. $\psi_i^E(\theta)$ is assumed to be a mirror image of $\psi_i^D(\theta)$ except for a lower height. $\psi_i^L(\theta)$ for different i are related by translation of $\pm 120^\circ$.

The overall potential energy $\Psi_0^{L1L2L3}(\theta)$ for γ rotation is assumed to be given by the simple sum of three energies:

$$\Psi_0^{L1L2L3}(\theta) = \psi_1^{L1}(\theta) + \psi_2^{L2}(\theta) + \psi_3^{L3}(\theta). \quad 5.$$

Experiments with a chimera of fast and slow βs indicate that, at least for kinetics, the properties of individual βs are additive (4). As seen in Figure 7*a* (*top*), the total potential energies in Equation 5 essentially reproduce the experimental potential diagram in Figure 4*d*: $\Psi_0^{TEE}(\theta)$, for example, represents the ATP-waiting state, and $\Psi_0^{TTE}(\theta)$ represents the state after ATP binding. In fact, the shape and height of the individual potential, $\psi_i^L(\theta)$, have been chosen arbitrarily, solely to reproduce the experimental diagram. The choice is nothing but one out of many possibilities that could underlie the experimental potentials.

In Figure 7*a* (*top*) and in all subsequent potential diagrams including Figure 7*b*, a constant is added to each potential energy such that each curve represents the free energy of the system including the motor and its environment. That is, starting from an arbitrarily chosen initial state, the following constants are added (subtracted for a reverse reaction) for every chemical transition in a β.

$$\mathrm{E} \rightarrow \mathrm{T}: -\ln K_{a0}^{ATP} - k_B T \ln[\mathrm{ATP}] \quad 6a.$$

$$\mathrm{T} \rightarrow \mathrm{H}: -\ln K_{hyd0} \quad 6b.$$

$$\mathrm{H} \rightarrow \mathrm{D}: -\ln K_{d0}^{Pi(1st)} + k_B T \ln[\mathrm{Pi}] \quad 6c.$$

$$\mathrm{H} \rightarrow \mathrm{P}: -\ln K_{d0}^{ADP(1st)} + k_B T \ln[\mathrm{ADP}] \quad 6d.$$

$$\mathrm{D} \rightarrow \mathrm{E}: -\ln K_{d0}^{ADP(2nd)} + k_B T \ln[\mathrm{ADP}] \quad 6e.$$

$$\mathrm{P} \rightarrow \mathrm{E}: -\ln K_{d0}^{Pi(2nd)} + k_B T \ln[\mathrm{Pi}], \quad 6f.$$

where K_0 is the equilibrium constant for the forward reactions (in the absence of the interaction between β and γ). These constants satisfy the conditions:

$$K_{a0}^{ATP} \cdot K_{hyd0} \cdot K_{d0}^{Pi(1st)} \cdot K_{d0}^{ADP(2nd)} = K_{a0}^{ATP} \cdot K_{hyd0} \cdot K_{d0}^{ADP(1st)} \cdot K_{d0}^{Pi(2nd)} = \exp(-\Delta G_0/k_B T), \quad 7.$$

where ΔG_0 is the standard free-energy change for ATP hydrolysis.

For example, starting from TEE, angle-dependent free energies for subsequent states are given by:

$$\Psi^{TEE}(\theta) = \Psi_0^{TEE}(\theta) \quad 8a.$$

$$\Psi^{TTE}(\theta) = \Psi_0^{TTE}(\theta) - \ln K_{a0}^{ATP} - k_B T \ln[ATP] \quad 8b.$$

$$\Psi^{HTE}(\theta) = \Psi_0^{HTE}(\theta) - \ln K_{a0}^{ATP} - k_B T \ln[ATP] - \ln K_{hyd0} \quad 8c.$$

$$\Psi^{DTE}(\theta) = \Psi_0^{DTE}(\theta) - \ln K_{a0}^{ATP} - k_B T \ln[ATP] - \ln K_{hyd0} - \ln K_{d0}^{Pi(1st)} + k_B T \ln[Pi] \quad 8d.$$

$$\Psi^{ETE}(\theta) = \Psi_0^{ETE}(\theta) - \ln K_{a0}^{ATP} - k_B T \ln[ATP] - \ln K_{hyd0} - \ln K_{d0}^{Pi(1st)} + k_B T \ln[Pi] - \ln K_{d0}^{ADP(2nd)} + k_B T \ln[ADP] \quad 8e.$$

$$= \Psi_0^{ETE}(\theta) + \Delta G_0 + k_B T \ln[ADP][Pi]/[ATP] \quad 8f.$$

$$= \Psi_0^{ETE}(\theta) + \Delta G. \quad 8g.$$

Note that $\Psi^{ETE}(\theta)$ for ETE obtained by unbinding of ATP from β_1 and binding of ATP to β_2 is given simply by $\Psi_0^{ETE}(\theta)$, which is $\Psi_0^{TEE}(\theta - 120^\circ)$, because hydrolysis is not involved.

For the equilibrium constants, we choose arbitrarily the following values: $K_{a0}^{ATP} = 6.1 \times 10^{11}\ M^{-1}$, $K_{hyd0} = 0.13$, $K_{d0}^{Pi(1st)} = 2.0 \times 10^{-3}$ M, $K_{d0}^{ADP(2nd)} = 1.5 \times 10^{-3}$ M, $K_{d0}^{ADP(1st)} = 1.0 \times 10^{-5}$ M, and $K_{d0}^{Pi(2nd)} = 0.31$ M. Note that these are just parameters and that actual equilibrium constants exhibit angle dependence determined by the difference between the initial and final $\psi(\theta)$s involved in the relevant chemical transition. For example, the affinity $K_{a1}^{ATP}(\theta)$ of β_1 for ATP is given by:

$$K_{a1}^{ATP}(\theta) = K_{a0}^{ATP} \cdot \exp\left\{\left[\psi_1^E(\theta) - \psi_1^T(\theta)\right]/k_B T\right\}, \quad 9.$$

which takes a maximal value of $6.7 \times 10^{14}\ M^{-1}$ at θ between -10° and 80° and a minimal value of $2.6\ M^{-1}$ at $\theta = 120^\circ$. The angle dependence can readily be appreciated from the vertical difference between the relevant two curves in Figure 7*a* (*top*). For example, $K_{hyd}(\theta)$, which is related to the difference between HTE and TTE curves, remains low and constant (=0.13) between -20° and 80°, and takes high values favoring hydrolysis between 80° and 120°, reaching a maximal value of 7.0×10^5 at 100°. Note that the angle-dependent equilibrium constants also satisfy Equation 7 at each angle. For example, to bind ADP (not ATP) and Pi from the medium for ATP synthesis, K_a^{ATP}, K_d^{ADP}, and K_d^{Pi} need all be small at some angle, which requires that K_{hyd} be large at the same angle. In our model, this happens around 90° for β_1.

Major Reaction Pathways

Now we discuss the rotation mechanism on the basis of the free-energy diagrams. In Figure 7*a* (top) we show the major reaction pathway at the indicated nucleotide concentrations. We choose TEE to be the starting state, where the potential minimum is at 0° and the motor waits for ATP at this angle. When ATP binds to the correct site (on β_2), the potential shifts to the red TTE curve. At 0°, however, the TTE curve is above the TEE curve, indicating that ATP binding is an uphill reaction. This is because the chosen ATP concentration, 2 μM, is low; the motor has to wait long for ATP to bind. The uphill part only poses a kinetic barrier, because as rotation proceeds the TTE curve becomes lower than TEE, stabilizing bound ATP. Indeed, Equation 8b indicates that the rate of passage over the (entropic) barrier at 0°, or the rate of ATP binding, should be proportional to [ATP], which is the expected kinetics. It is possible, however, that the motor binds ATP by crossing from TEE to TTE around 15°, where the barrier height is lower. This could happen through thermal fluctuation of the γ angle, and the rate of ATP binding would no longer be proportional to [ATP]; kinetic barrier in this pathway is actually high, because ATP must arrive at the moment where γ happens to fluctuate counterclockwise by $\sim$15°. Experimentally, the stepping rate of the F_1 motor is proportional to [ATP] down to $<$1 nM, suggesting that ATP binding occurs by an upward jump from TEE to TTE. The rate of binding of a fluorescent ATP analog indeed becomes lower when γ is rotated slightly counterclockwise from an ATP-waiting angle (K. Adachi, unpublished data). It seems that closure of the binding site poses a kinetic barrier and impedes binding, in addition to stabilizing a bound nucleotide; higher affinity for ATP upon counterclockwise rotation results from decrease in the rate of ATP release.

Once ATP is bound, the motor slides down the slope of the TTE curve to 80°, producing an apparent torque of $\sim$50 pN $\cdot$ nm. That is, an actin filament or bead attached to γ can be rotated at a speed commensurate with this much torque (Equation 4). Note that in the world of molecular machines, mass is negligible, or motion is always overdamped, and thus a linear potential produces motion at a constant speed. When γ reaches 80°, the motor again waits for thermal activation to hydrolyze ATP and, upon activation, switches onto the HTE curve to reach 90°. One of the two experimentally observed $\sim$1 ms reactions around 90° likely corresponds to this process. At 90°, both PTE and DTE curves are below the HTE curve, because [ADP] and [Pi] are low in this diagram, and thus either ADP or Pi is readily released. The ETE curve is further below, and the motor lands on this curve by releasing the last hydrolysis product. The last 30° is again a torque-generating downhill process, except for the first 10°, which is slightly uphill and which might correspond to the observed second $\sim$1 ms reaction. At 120°, the motor waits for the next ATP.

In our scheme, torque is given as the slope of the potential energy, which is an intrinsic property of the motor. Thus, the torque is independent of speed or nucleotide concentrations. A cargo attached to the rotor rotates at a speed commensurate

with Equation 4, as long as internal impeding factors such as friction are negligible. Indeed, the apparent torque calculated from Equation 4 is independent of [ATP] and of speed up to ~30 revolutions s^{-1}, compared with the full speed of 130 revolutions s^{-1} (64, 65): Internal friction does not manifest its effect up to one fourth of the maximal speed. Another rotary motor, the flagellar motor that is driven by proton flow, also shows nearly speed-independent torque at low speeds (5).

Other Pathways

We consider five chemical states, T, H, D, P, and E, for each β, and thus there are a total of 125 chemical states, each associated with a unique potential energy, $\Psi_0(\theta)$. More states would appear in our free-energy diagram showing $\Psi(\theta)$s, in which the same chemical state can have a different vertical offset, in multiples of ΔG, depending on the net number of ATP hydrolyzed/synthesized to reach that state. In Figure 7*a* (*top*) we present only five of these $\Psi(\theta)$s. Now we show that these indeed constitute the major pathway, at least at moderate concentrations of nucleotides.

In Figure 7*b* we show all states that are accessible from TEE (*bottom*) or TTE (*top*): Destinations from T are E (unbinding) or H (hydrolysis), and destinations from E are T, D, or P (all bindings). From TEE at 0° (an ATP-waiting state), TTE at 80° is the most likely destination because the barrier to TTE is low (almost absent at the indicated ATP concentration) and the minimum of TTE at 80° is the lowest. This is why we show the path TEE → TTE as the major pathway in Figure 7*a* (*top*). The other, equally stable destination is TET at −40° (binding to the wrong site), but a high barrier exists because β_3 is fully unbent and its affinity for ATP is low. Binding of ATP to this wrong site could still happen rarely and might account for occasional backward 120° steps observed at low ATP concentrations (64). In the model, however, the major path from TET at −40° is to return to TEE at 0°, without hydrolysis of ATP. Completion of a backward 120° step through hydrolysis of ATP, i.e., reaching EET at −120° through HET and DET, is a minor path.

Another path from TEE at 0° is toward HEE at 0° (hydrolysis without rotation). Because the barrier to HEE is only a few k_BT high, the motor fluctuates between the two states, or ATP and ADP + Pi are near equilibrium at 0°. This can account for the extensive exchange of Pi oxygens during catalysis at low [ATP] (10). From HEE, there is another pathway to EEE through DEE or PEE. This is the so-called uni-site catalysis (26) and does not accompany rotation in our model, in accord with the experiment showing ATP hydrolysis in F_1 in which γ is cross-linked to β (14).

Thus, although the pathway shown in Figure 7*a* (*top*) is the major one in that it crosses the lowest barriers and follows free-energy minima, there are many other paths that can be populated to some extent. Some are just detours that return to the major pathway without expenditure of ATP, as in the example of TEE → TET → TEE or TEE → HEE → TEE. Others constitute uncoupled pathways in

which ATP hydrolysis occurs without rotation, such as the uni-site hydrolysis or reverse rotation failing to synthesize ATP (see below). It is also possible that a forward 120° step is made without expending ATP, as in the example of TEE to ETE simply by binding and unbinding of ATP. A backward 120° step, however, occurs through an equivalent sequence toward EET, with the same (and small) probability: On the free-energy diagram the three states, TEE, ETE, and EET, are related by a purely horizontal 120° shift unless ATP hydrolysis or synthesis is involved. Naturally, there is no unidirectional motion without expenditure of free energy. The extent to which the nonmajor pathways are populated depends on the rate constants of chemical reactions and rotation. We do not discuss kinetics here because too many angle-dependent rates are involved and most are experimentally unknown. Formalisms for kinetic analysis are given in References 44 and 57.

EFFICIENCY OF CHEMO-MECHANICAL ENERGY CONVERSION

Hereafter, we focus on the major pathway shown in Figure 7*a* (*top*), and we further neglect PTE to simplify the diagram. The discussion below is based on free-energy diagrams that are basically experimental, and does not depend on the details of the model, such as whether it operates in the bi-site or tri-site scheme. TEE implies an ATP-waiting state, TTE the state after ATP binding (to an unspecified site), HTE after hydrolysis of ATP (in an unspecified site), DTE after Pi release, and ETE the ATP-waiting state after a 120° step accompanying hydrolysis of one ATP molecule has occurred. An alternative representation for a tri-site pathway, among others, is TED → TTD → TTE → HTE → DTE, which is similar to the bi-site scheme except that the last 30(40)° substep is driven by Pi release and that ADP stays on F_1 until prompted by subsequent ATP binding (Figure 4*c*′). Another, more genuine tri-site scheme is TEH → TTH → HTH → HTD → HTE, in which ATP binds to β_2, hydrolysis occurs in β_1, and product release is from β_3.

Responses to Decreasing ΔG in the Absence of External Load

Figure 8*a* shows a free-energy diagram for nucleotide concentrations at which the free energy decreases relatively smoothly and linearly as rotation proceeds. When a large cargo such as an actin filament or bead is attached to γ, the motor will do an apparent work of ∼100 pN · nm or 25 k_BT per 120° step against the viscous load, which is approximately equal to the free-energy input, ΔG, under the chosen conditions. The situation, however, is different from work against a conservative force (see below), and the cargo simply stirs the solution, producing heat. Net heat production per ATP hydrolyzed, including the heat associated with the chemical reactions and possible loans from the environment, is not 100 pN · nm and is given by $-\Delta H$, which is ∼45 pN · nm at pH 7 (28). The heat output is independent of ΔG or of whether a cargo is attached to γ, unless the motor does work against a conservative force.

Now we reduce ΔG, first by decreasing [ATP] (Figure 8*b*). In the free-energy diagram, all curves after ATP binding are brought up by the term $-k_BT$ ln[ATP] (Equations 8b–e). ATP binding is now uphill, and the motor must borrow some free energy (negative entropy) from the environment. That is, the motor must wait at $\sim 0^\circ$ for the rare event of ATP binding.

We can further reduce ΔG by increasing [ADP] and [Pi] (Figure 8*c*). Then the curve DTE is brought up by the term k_BT ln[Pi], and ETE is further brought up by the term k_BT ln[ADP]. The result is that both Pi and ADP releases are uphill: Immediate rebinding occurs in proportion to [Pi] and [ADP], which are both high. Thus, the motor cannot readily release the products and would dwell around 90°. However, in the rare event that the motor happens to release both products, rotate to $\sim 120^\circ$, and bind a next ATP, it can proceed onto the curve ETT and reach 200° (dashed curve in Figure 8*c*). Although the probability of the forward stepping should be extremely low under the chosen conditions, it is still much higher than the reaction back to TEE at 0°. As long as ΔG is negative, the motor eventually rotates counterclockwise however rarely it may step.

Changes in the rates of ATP binding and product rebinding enable the motor to "sense" the nucleotide concentrations, or free energy of the environment. Note that, irrespective of ΔG, rotation occurs along the same slopes and thus at the same speed. If one calculated the amount of apparent work from the rotary speed during forward stepping, it would still be ~ 100 pN $\cdot$ nm, whereas ΔG is only about -20 pN $\cdot$ nm in Figure 8*c*. The apparent efficiency could thus exceed 100%. Thermodynamic efficiency, however, has to be discussed for the situation when a motor works against a conservative force that pushes back the motor (see below). To deal with the case of viscous load, the concept of generalized efficiency has been introduced (69) and developed as Stokes efficiency (58), which is based on the rotary speed averaged over a long time including interstep dwells and which is bound by 100%; for a high Stokes efficiency, the motor torque must be angle-independent, as in the F_1 motor. Experiments at varying [ATP] have shown that the apparent amount of work in a 120° step is independent of [ATP], as discussed above (64). Experiments at high [ADP] are difficult because of the MgADP inhibition.

Rotation Against a Conservative Force

A different scenario arises when an external torque is applied to the motor. A conservative torque, such as one exerted by a magnet or bent actin, operates on a motor regardless of whether the motor is moving. The magnitude of torque depends on the motor angle, not speed. In contrast, the viscous torque disappears when the motor stops. The viscous torque impedes motor movement, but it never pushes back the motor, whereas a conservative torque does.

Below we examine the case of angle-independent external torque (Figure 8*d–i*). The torque F_o applies on F_1 is expected to be relatively smooth, because the rotor of F_o possesses 10- to 14-fold symmetry (13a, 53, 67). An externally applied force on a linear molecular motor, e.g., with an optical trap, is practically constant over the size of the motor step.

Figure 8*d–f* shows diagrams of free energy (including the potential energy of the external torque) at increasing opposing torque for the nucleotide concentrations in Figure 8*a*. As seen, the motor moves forward (counterclockwise) as long as the total free energy decreases over a 120° step (TEE → ETE), or as long as $\Delta G + W$ is negative, where $W\,(>0)$ is the work done against the external opposing torque $N_{\rm ext}$ ($W = N_{\rm ext} \cdot 2\pi/3$). That is, the motor can do positive work (output) up to the amount, $-\Delta G$ (input), determined by the nucleotide concentrations. When W exceeds $-\Delta G$ (Figure 8*f*), the motor rotates in reverse, pushed by the external torque. The reverse rotation leads to ATP synthesis, basically in the sequence ETE → DTE → HTE → TTE → TEE, although under the conditions of Figure 8*f*, the motor tends to hop between these states. A more comfortable situation for synthesis is shown in Figure 8*g*, in which the above sequence is almost guaranteed (thanks to the higher concentrations of ADP and Pi).

Here we discuss the efficiency of chemo-mechanical energy conversion, first considering solely the major pathway; the discussion ignoring uncoupled pathways sets an upper limit for the efficiency. For forward rotation, the input is $-\Delta G$, which is determined by nucleotide concentrations, and the output is W, which is determined by the external torque. The efficiency of chemical to mechanical energy conversion would thus apparently be $W/|\Delta G|$, which is independent of the motor properties except for the step size. The efficiency would approach 100% as W and $|\Delta G|$ become comparable. When W equals $|\Delta G|$, the motor fluctuates equally in both directions, hydrolyzing and resynthesizing ATP. When $W > |\Delta G|$, the efficiency of mechanical to chemical energy conversion (ATP synthesis) would be given by $|\Delta G|/W$, again independent of motor properties. When $W < |\Delta G|$, the difference is dissipated as an increase in entropy (and heat if $W < |\Delta H| = 45\ \mathrm{pN \cdot nm}$). When $W > |\Delta H|$, the difference in energy is supplied, in the form of heat, by the environment as the heat bath.

According to the argument above, a motor would always achieve 100% efficiency when W equals $|\Delta G|$. In fact, there are many uncoupled pathways that reduce the efficiency and that critically depend on the make of a particular motor. The efficiency above, $W/|\Delta G|$ or $|\Delta G|/W$, is thus an upper limit. Actual efficiency depends on kinetic parameters (rate constants) that dictate the probabilities of branching among various pathways.

Uncoupling scenarios can be seen even on a diagram depicting the major pathway. In Figure 8*f*, for example, there is a possibility that the motor, starting on the ETE curve at 120°, slides along the ETE line toward the left without picking up ADP and Pi. It encounters a small barrier at 0°, but there is a certain probability that the motor crosses the barrier toward left. That is, an external torque may simply rotate the motor clockwise without synthesizing ATP. The probability of this scenario is high under a higher torque, as one expects: If one rotates the motor too fast, the motor will certainly fail to pick up ADP and Pi or to synthesize ATP.

Another example is given in Figure 8*h*, in which $|\Delta G|$ is quite large (136 $\mathrm{pN \cdot nm}$) and might be expected to drive counterclockwise rotation against the large external torque of 60 $\mathrm{pN \cdot nm}$ ($W = 123\ \mathrm{pN \cdot nm}$). The shape of the TEE (or ETE)

curve, however, is such that the motor yields to the external torque and tends to rotate clockwise without hydrolyzing or synthesizing ATP. There must be an upper limit to the force (torque) a motor can produce, and it is about 50 pN · nm for this particular motor. Near the upper limit, the tendency toward uncoupled, backward motion increases, as seen in Figure 8*e*. One cannot let a motor do an arbitrarily large amount of work by increasing $|\Delta G|$. "Give" (yielding under a high backward force) is a common phenomenon for linear molecular motors in an optical trap (33, 54).

Dissipation and Friction

Let us confine the discussion to the case of coupling ratio being close to 1 (see Reference 46 for more general discussion). Then, the efficiency is close to $W/|\Delta G|$ or $|\Delta G|/W$, determined by $|\Delta G|$ and W alone. This implies that the magnitude of friction, internal or external, has little effect on the efficiency. A poorly designed motor with high internal friction simply runs slowly, with the same efficiency as a low friction motor. The efficiency also remains the same if an external friction is added, by attaching a large cargo to the rotor. The cargo only slows down the motor.

One might think that dissipation could occur via free-energy drop without motor motion, such as the initial ATP binding, before subsequent rotation, at high [ATP]. In Figure 9*a*, for example, the overall ΔG is assumed to be the same as in Figure 8*a*, but [ATP] (or K_{a0}^{ATP}) is set high and [ADP] (or K_{d0}^{ADP}) is set correspondingly low. Thus, ATP binding (downward arrow) dissipates free energy because no work is done during the binding, except for the internal work on the protein machine that is independent of [ATP]. The dissipation, however, is canceled at the moment of ADP binding (upward arrow), which is now uphill and requires a loan of free energy from the environment. Again, the overall efficiency is unchanged, although the motor runs slower because of the uphill portion.

HOW TO DESIGN AN ATP-DRIVEN MOLECULAR MACHINE

In principle, one could conceive of a motor that makes multiple steps per ATP hydrolyzed (27); the motor could even be smart enough to make only one step under a high load to produce a correspondingly high force. Though attractive, working out a possible, reasonably detailed design for such a motor is not easy for us. We therefore restrict our discussion to one-step motors.

We presume that the most desirable characteristics of a molecular machine are high efficiency of energy conversion and high speed. If so, the design shown in Figure 8 is close to ideal, as an ATP-driven rotary motor under the nucleotide concentrations of Figure 8*a*, *d–f* and as a torque-driven ATP synthesizer under the nucleotide concentrations of Figure 8*g*.

Linear potentials that produce angle-independent torque, or position-independent force for a linear motor, are better than curved potentials. Figure 9*b*, for

example, shows parabolic potentials (solid lines), which may be expected for a linear molecular motor (such as kinesin) that makes a diffusional search (shallow potential on the left) followed by binding to a specific site (deep potential on the right). Such a design, however, suffers from extreme slowing down in the presence of an opposing load, because the barrier between the two potentials rises sharply (dotted lines). Linear potentials do not suffer from this effect (Figure 8*d–f*). Linear potentials are also advantageous when a molecular machine is to be driven by an external force (Figure 8*f*), because they allow smooth, less bumpy and thus faster motion.

To obtain a high efficiency of energy conversion at a high speed, free energy must decrease smoothly, as in Figure 8*a*, without an uphill portion that degrades speed and without a vertical drop that degrades the efficiency. Even with a well-designed motor, however, these conditions are met only under one specific set of nucleotide concentrations. In other words, a molecular machine must be designed to work best in its working environment; its performance drops in other environments.

If one is to avoid uncoupling, or give, at a high load, one needs a barrier(s) against uncoupled pathways. This problem is serious for a machine to be driven by an external force, such as the ATP synthase. Potential diagrams that are too smooth, such as those in Figure 8*f* or 8*h*, are liable to uncoupling. Ideally, barriers should be introduced in positions outside the normal pathway, such as the small bumps around -20° in Figure 8*f*. An arbitrarily high barrier, however, cannot be introduced, because it must disappear in another chemical state (to let the motor cross that point); the appearance/disappearance of the barrier must be driven by a chemical reaction with a limited drop in free energy. A solution that sacrifices speed is to allow the presence of some bumps or uphill portions in the major pathway, as in Figure 8*g*. A highly bumpy diagram, as shown in Figure 8*i*, warrants tight coupling (and ~100% energy-conversion efficiency near the balancing $|\Delta G|$, which is 30 pN · nm in Figure 8*i*), although speed is greatly reduced.

The free-energy diagrams in Figure 8 are derived from the experimental potential energies in the actual F_1 motor, with equilibrium constants chosen to mimic, approximately, the behavior of F_1 under a variety of nucleotide concentrations. It seems that the F_1 motor is designed to be an almost ideal ATP synthesizer working under physiological conditions when driven by moderate torque (Figure 8*g*). For ATP-driven rotation, fast operation requires a relatively low [ADP] (Figure 8*a*), which is a condition adopted in in vitro studies. If the motor is to work as an ion pump in vivo, as with V_oV_1-ATPase, effective K_d^{ADP} needs to be increased.

ACKNOWLEDGMENTS

We thank members of the Kinosita lab and the former CREST Team 13 for collaboration and discussion. Critical comments by Y. Oono (University of Illinois), E. Muneyuki (Tokyo Institute of Technology), and H. Nakanishi (Kyushu University) are particularly appreciated. This work was supported by Grants-in-Aid from the Ministry of Education, Culture, Sports, Science and Technology of Japan.

The *Annual Review of Biophysics and Biomolecular Structure* is online at http://biophys.annualreviews.org

LITERATURE CITED

1. Abrahams JP, Leslie AGW, Lutter R, Walker JE. 1994. Structure at 2.8 Å resolution of F_1-ATPase from bovine heart mitochondria. *Nature* 370:621–28
2. Adachi K, Noji H, Kinosita K Jr. 2003. Single-molecule imaging of rotation of F_1-ATPase. *Methods Enzymol.* 361:211–27

2a. Adachi K, Yasuda R, Noji H, Itoh H, Harada Y, et al. 2000. Stepping rotation of F_1-ATPase visualized through angle-resolved single-fluorophore imaging. *Proc. Natl. Acad. Sci. USA* 97:7243–47

3. Antes I, Chandler D, Wang H, Oster G. 2003. The unbinding of ATP from F_1-ATPase. *Biophys. J.* 85:695–706
4. Ariga T, Masaike T, Noji H, Yoshida M. 2002. Stepping rotation of F_1-ATPase with one, two, or three altered catalytic sites that bind ATP only slowly. *J. Biol. Chem.* 277:24870–74
5. Berg HC. 2003. The rotary motor of bacterial flagella. *Annu. Rev. Biochem.* 72:19–54
6. Berg JM, Tymoczko JL, Stryer L. 2001. *Biochemistry.* New York: Freeman. 974 pp. 5th ed.
7. Böckmann RA, Grubmüller H. 2002. Nanoseconds molecular dynamics simulation of primary mechanical energy transfer steps in F_1-ATP synthase. *Nat. Struct. Biol.* 9:198–202
8. Böckmann RA, Grubmüller H. 2003. Conformational dynamics of the F_1-ATPase β-subunit: a molecular dynamics study. *Biophys. J.* 85:1482–91
9. Börsch M, Diez M, Zimmermann B, Reuter R, Gräber P. 2002. Stepwise rotation of the γ-subunit of EF_oF_1-ATP synthase observed by intramolecular single-molecule fluorescence resonance energy transfer. *FEBS Lett.* 527:147–52

9a. Börsch M, Diez M, Zimmermann B, Trost M, Steigmiller S, Gräber P. 2003. Stepwise rotation of the γ-subunit of EF_oF_1-ATP synthase during ATP synthesis: a single-molecule FRET approach. *Proc. SPIE* 4962:11–21

10. Boyer PD. 1997. The ATP synthase: a splendid molecular machine. *Annu. Rev. Biochem.* 66:717–49
11. Boyer PD. 2002. Catalytic site occupancy during ATP synthase catalysis. *FEBS Lett.* 512:29–32
12. Boyer PD, Kohlbrenner WE. 1981. The present status of the binding-change mechanism and its relation to ATP formation by chloroplasts. In *Energy Coupling in Photosynthesis*, ed. BR Selman, S Selman-Reimer, pp. 231–40. Amsterdam: Elsevier
13. Dittrich M, Hayashi S, Schulten K. 2003. On the mechanism of ATP hydrolysis in F_1-ATPase. *Biophys. J.* 85:2253–66

13a. Fillingame RH, Angevine CM, Dmitriev OY. 2003. Mechanics of coupling proton movements to *c*-ring rotation in ATP synthase. *FEBS Lett.* 555:29–34

14. García JJ, Capaldi RA. 1998. Unisite catalysis without rotation of the γ-ε domain in *Escherichia coli* F_1-ATPase. *J. Biol. Chem.* 273:15940–45
15. Gibbons C, Montgomery MG, Leslie AGW, Walker JE. 2000. The structure of the central stalk in bovine F_1-ATPase at 2.4 Å resolution. *Nat. Struct. Biol.* 7:1055–61
16. Hara KY, Noji H, Bald D, Yasuda R, Kinosita K Jr, Yoshida M. 2000. The role of the DELSEED motif of the β subunit in rotation of F_1-ATPase. *J. Biol. Chem.* 275:14260–63
17. Hayashi S, Oda N, Oosawa F. 1982. A loose coupling model of H^+-ATPase. *Proc. 20th Annu. Meet. Biophys. Soc. Jpn.* p. 119. (Abstr.)

18. Hirono-Hara Y, Noji H, Nishiura M, Muneyuki E, Hara KY, et al. 2001. Pause and rotation of F_1-ATPase during catalysis. *Proc. Natl. Acad. Sci. USA* 98:13649–54
19. Hisabori T, Kondoh A, Yoshida M. 1999. The γ subunit in chloroplast F_1-ATPase can rotate in a unidirectional and counterclockwise manner. *FEBS Lett.* 463:35–38
20. Hunt AJ, Gittes F, Howard J. 1994. The force exerted by a single kinesin molecule against a viscous load. *Biophys. J.* 67:766–81
21. Imamura H, Nakano M, Noji H, Muneyuki E, Ohkuma S, et al. 2003. Evidence for rotation of V_1-ATPase. *Proc. Natl. Acad. Sci. USA* 100:2312–15
22. Itoh H, Takahashi A, Adachi K, Noji H, Yasuda R, et al. 2004. Mechanically driven ATP synthesis by F_1-ATPase. *Nature.* 427:465–68
23. Jault JM, Dou C, Grodsky NB, Matsui T, Yoshida M, Allison WS. 1996. The $\alpha_3\beta_3\gamma$ subcomplex of the F_1-ATPase from the thermophilic *Bacillus* PS3 with the βT165S substitution does not entrap inhibitory MgADP in a catalytic site during turnover. *J. Biol. Chem.* 271:28818–24
24. Kato-Yamada Y, Noji H, Yasuda R, Kinosita K Jr, Yoshida M. 1998. Direct observation of the rotation of ε subunit in F_1-ATPase. *J. Biol. Chem.* 273:19375–77
25. Kinosita K Jr, Yasuda R, Noji H. 2000. F_1-ATPase: a highly efficient rotary ATP machine. *Essays Biochem.* 35:3–18
26. Kinosita K Jr, Yasuda R, Noji H, Adachi K. 2000. A rotary molecular motor that can work at near 100% efficiency. *Philos. Trans. R. Soc. London Sci. Ser. B* 355:473–89
27. Kitamura K, Tokunaga M, Iwane AH, Yanagida T. 1999. A single myosin head moves along an actin filament with regular steps of 5.3 nanometres. *Nature* 397:129–34
28. Kodama T. 1985. Thermodynamic analysis of muscle ATPase mechanisms. *Physiol. Rev.* 65:467–551
29. Ma J, Flynn TC, Cui Q, Leslie AGW, Walker JE, Karplus M. 2002. A dynamic analysis of the rotation mechanism for conformational change in F_1-ATPase. *Structure* 10:921–31
30. Mannherz HG, Schenck H, Goody RS. 1974. Synthesis of ATP from ADP and inorganic phosphate at the myosin-subfragment 1 active site. *Eur. J. Biochem.* 48:287–95
31. Masaike T, Muneyuki E, Noji H, Kinosita K Jr, Yoshida M. 2002. F_1-ATPase changes its conformations upon phosphate release. *J. Biol. Chem.* 277:21643–49
32. Matsui T, Muneyuki E, Honda M, Allison WS, Dou C, Yoshida M. 1997. Catalytic activity of the $\alpha_3\beta_3\gamma$ complex of F_1-ATPase without noncatalytic nucleotide binding site. *J. Biol. Chem.* 272:8215–21
33. Mehta AD, Rock RS, Rief M, Spudich JA, Mooseker MS, Cheney RE. 1999. Myosin-V is a processive actin-based motor. *Nature* 400:590–93
34. Menz RI, Walker JE, Leslie AGW. 2001. Structure of bovine mitochondrial F_1-ATPase with nucleotide bound to all three catalytic sites: implications for the mechanism of rotary catalysis. *Cell* 106:331–41
35. Milgrom YM, Murataliev MB, Boyer PD. 1998. Bi-site activation occurs with the native and nucleotide-depleted mitochondrial F_1-ATPase. *Biochem. J.* 330:1037–43
36. Müller M, Pänke O, Junge W, Engelbrecht S. 2002. F_1-ATPase, the C-terminal end of subunit γ is not required for ATP hydrolysis-driven rotation. *J. Biol. Chem.* 277:23308–13
37. Nishio K, Iwamoto -Kihara A, Yamamoto A, Wada Y, Futai M. 2002. Subunit rotation of ATP synthase embedded in membranes: *a* or β subunit rotation relative to the *c* subunit ring. *Proc. Natl. Acad. Sci. USA* 99:13448–52
37a. Nishizaka T, Oiwa K, Noji H, Kimura S, Muneyuki E, et al. 2004. Chemomechanical coupling in F_1-ATPase

revealed by simultaneous observation of nucleotide kinetics and rotation. *Nature Struct. Mol. Biol.* 11:142–48

38. Noji H, Bald D, Yasuda R, Itoh H, Yoshida M, Kinosita K Jr. 2001. Purine but not pyrimidine nucleotides support rotation of F_1-ATPase. *J. Biol. Chem.* 276:25480–86
39. Noji H, Häsler K, Junge W, Kinosita K Jr, Yoshida M, Engelbrecht S. 1999. Rotation of *Escherichia coli* F_1-ATPase. *Biochem. Biophys. Res. Commun.* 260:597–99
40. Noji H, Yasuda R, Yoshida M, Kinosita K Jr. 1997. Direct observation of the rotation of F_1-ATPase. *Nature* 386:299–302
41. Omote H, Sambonmatsu N, Saito K, Sambongi Y, Iwamoto-Kihara A, et al. 1999. The γ-subunit rotation and torque generation in F_1-ATPase from wild-type or uncoupled mutant *Escherichia coli*. *Proc. Natl. Acad. Sci. USA* 96:7780–84
42. Ono S, Hara KY, Hirao J, Matsui T, Noji H, Yoshida M, Muneyuki E. 2003. Origin of apparent negative cooperativity of F_1-ATPase. *Biochim. Biophys. Acta* 1607:35–44
43. Oosawa F, Hayashi S. 1983. Coupling between flagellar motor rotation and proton flux in bacteria. *J. Phys. Soc. Jpn.* 52:4019–28
44. Oosawa F, Hayashi S. 1986. The loose coupling mechanism in molecular machines of living cells. *Adv. Biophys.* 22:151–83
45. Pänke O, Cherepanov DA, Gumbiowski K, Engelbrecht S, Junge W. 2001. Viscoelastic dynamics of actin filaments coupled to rotary F-ATPase: angular torque profile of the enzyme. *Biophys. J.* 81:1220–33
46. Parmeggiani A, Jülicher F, Ajdari A, Prost J. 1999. Energy transduction of isothermal ratchets: generic aspects and specific examples close to and far from equilibrium. *Phys. Rev. E* 60:2127–40
47. Ren H, Allison WS. 2000. Substitution of βGlu^{201} in the $\alpha_3\beta_3\gamma$ subcomplex of the F_1-ATPase from the thermophilic *Bacillus* PS3 increases the affinity of catalytic sites for nucleotides. *J. Biol. Chem.* 275:10057–63
48. Sakamoto J. 1984. Effect of dimethylsulfoxide on ATP synthesis by mitochondrial soluble F_1-ATPase. *J. Biochem.* 96:483–87
49. Sambongi Y, Iko Y, Tanabe M, Omote H, Iwamoto-Kihara A, et al. 1999. Mechanical rotation of the c subunit oligomer in ATP synthase (F_oF_1): direct observation. *Science* 286:1722–24
50. Shimabukuro K, Yasuda R, Muneyuki E, Hara KY, Kinosita K Jr, Yoshida M. 2003. Catalysis and rotation of F_1 motor: cleavage of ATP at the catalytic site occurs in 1 ms before 40° substep rotation. *Proc. Natl. Acad. Sci. USA.* 100:14731–36
51. Shirakihara Y, Leslie AGW, Abrahams JP, Walker JE, Ueda T, et al. 1997. The crystal structure of the nucleotide-free $\alpha_3\beta_3$ subcomplex of F_1-ATPase from the thermophilic *Bacillus PS3* is a symmetric trimer. *Structure* 5:825–36
52. Soong RK, Bachand GD, Neves HP, Olkhovets AG, Craighead HG, Montemagno CD. 2000. Powering an inorganic nanodevice with a biomolecular motor. *Science* 290:1555–58
53. Stock D, Leslie AGW, Walker JE. 1999. Molecular architecture of the rotary motor in ATP synthase. *Science* 286:1700–5
54. Svoboda K, Schmidt CF, Schnapp BJ, Block SM. 1993. Direct observation of kinesin stepping by optical trapping interferometry. *Nature* 365:721–27
55. Tsunoda SP, Aggeler R, Noji H, Kinosita K Jr, Yoshida M, Capaldi RA. 2000. Observations of rotation within the F_oF_1-ATP synthase: deciding between rotation of the F_oc subunit ring and artifact. *FEBS Lett.* 470:244–48
56. Turina P, Samoray D, Gräber P. 2003. H^+/ATP ratio of proton transport-coupled ATP synthesis and hydrolysis catalysed by CF_oF_1-liposomes. *EMBO J.* 22:418–26
57. Wang H, Oster G. 1998. Energy transduction in the F_1 motor of ATP synthase. *Nature* 396:279–82

58. Wang H, Oster G. 2002. The Stokes efficiency for molecular motors and its applications. *Europhys. Lett.* 57:134–40
59. Weber J, Senior AE. 2001. Bi-site catalysis in F_1-ATPase: Does it exist? *J. Biol. Chem.* 276:35422–28
60. Weber J, Senior AE. 2003. ATP synthesis driven by proton transport in F_1F_0-ATP synthase. *FEBS Lett.* 545:61–70
61. Wolcott RG, Boyer PD. 1974. The reversal of the myosin and actomyosin ATPase reactions and the free energy of ATP binding to myosin. *Biochem. Biophys. Res. Commun.* 57:709–16
62. Yagi H, Tozawa K, Sekino N, Iwabuchi T, Yoshida M, Akutsu H. 1999. Functional conformation changes in the TF_1-ATPase β subunit probed by 12 tyrosine residues. *Biophys. J.* 77:2175–83
63. Yasuda R, Masaike T, Adachi K, Noji H, Itoh H, Kinosita K Jr. 2003. The ATP-waiting conformation of rotating F_1-ATPase revealed by single-pair fluorescence resonance energy transfer. *Proc. Natl. Acad. Sci. USA* 100:9314–18
64. Yasuda R, Noji H, Kinosita K Jr, Yoshida M. 1998. F_1-ATPase is a highly efficient molecular motor that rotates with discrete 120° steps. *Cell* 93:1117–24
65. Yasuda R, Noji H, Yoshida M, Kinosita K Jr, Itoh H. 2001. Resolution of distinct rotational substeps by submillisecond kinetic analysis of F_1-ATPase. *Nature* 410:898–904
66. Yoshida M. 1983. The synthesis of enzyme-bound ATP by the F_1-ATPase from the thermophilic bacterium PS3 in 50% dimethylsulfoxide. *Biochem. Biophys. Res. Commun.* 114:907–12
67. Yoshida M, Muneyuki E, Hisabori T. 2001. ATP synthase—a marvellous rotary engine of the cell. *Nat. Rev. Mol. Cell Biol.* 2:669–77
68. Zhou Y, Duncan TM, Cross RL. 1997. Subunit rotation in *Escherichia coli* F_oF_1-ATP synthase during oxidative phosphorylation. *Proc. Natl. Acad. Sci. USA* 94: 10583–87
69. Derényi I, Bier M, Astumian RD. 1999. Generalized efficiency and its application to microscopic engines. *Phys. Rev. Lett.* 83:903–6
70. Diez M, Zimmermann B, Börsch M, König M, Schweinberger E, et al. 2004. Proton-powered subunit rotation in single membrane-bound F_0F_1-ATP synthase. *Nat. Struct. Mol. Biol.* 11:135–41

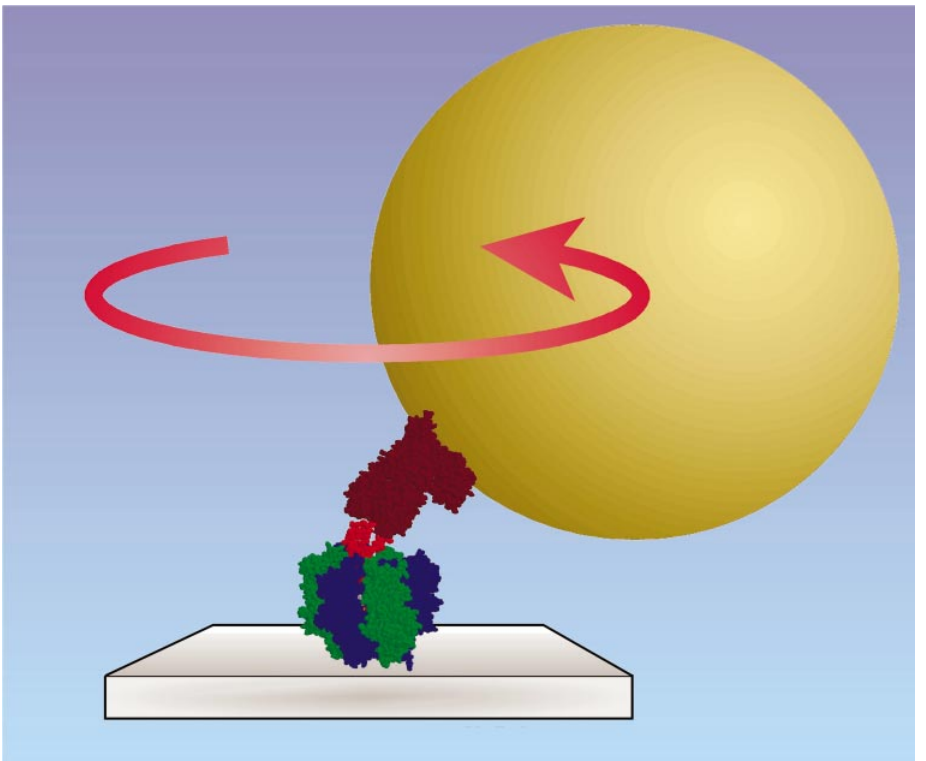

Figure 1 Observation of F_1 rotation (65). Three β subunits (*green*) were attached to a glass surface through histidine residues engineered on the N terminus. To the central γ subunit (*red*), a 40-nm gold bead was attached through BSA and streptavidin (both *brown*). Rotation was observed by dark-field microscopy. A larger bead can be observed under an ordinary microscope, and a fluorescent actin filament attached to γ was observed under a fluorescence microscope (40). The α subunit is in blue. The 40-nm bead and proteins in the figure are approximately to scale.

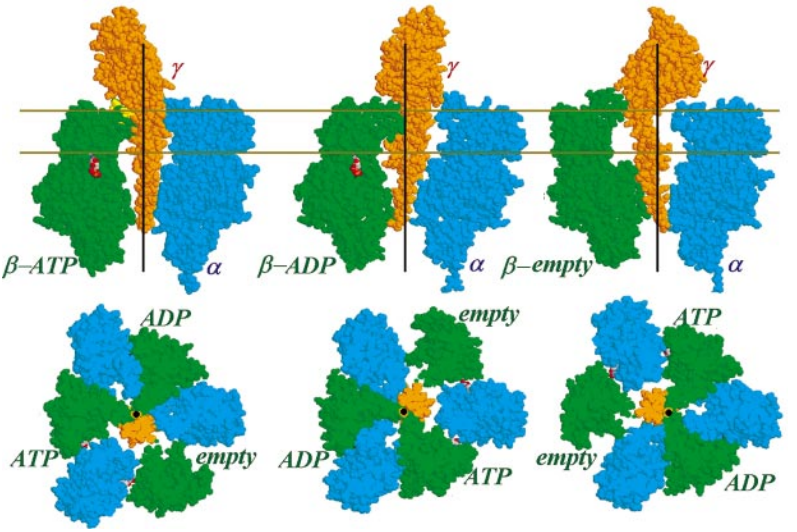

Figure 2 A crystal structure of mitochondrial F_1 (15). α subunits, light-blue; β subunits, green (DELSEED motif in yellow at upper left); γ subunit, orange. Of the three catalytic sites, each being at an α-β interface but hosted mainly by the β, two bind MgADP and the third is empty. In another, quite similar structure (1), one β carries an ATP analog instead of ADP, and thus that β is designated β-ATP. *Top*: Three vertical sections rotated by 120° with respect to each other. *Bottom*: Corresponding horizontal sections between gold lines at top. Black lines at top and black dots at bottom represent the putative axis of γ rotation (57).

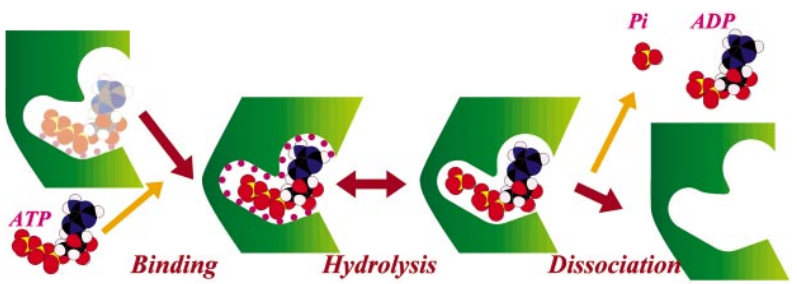

Figure 5 How an ATP-driven molecular machine may work. An ATPase protein (shown in *green*) does work by changing its conformation. In this example, the protein bends when it binds ATP and unbends upon release of hydrolysis products. Brown arrows indicate how free energy decreases, accompanying work output, during the reaction. Major work is done in the process of ATP binding (and product release), not much in conjunction with hydrolysis. Violet dots represent bonds between ATP and the protein. Light-colored ATP on the left represents the state after initial binding. The ATP pulls and bends the protein by progressively making more bonds while the ATP is bound more tightly by the protein.

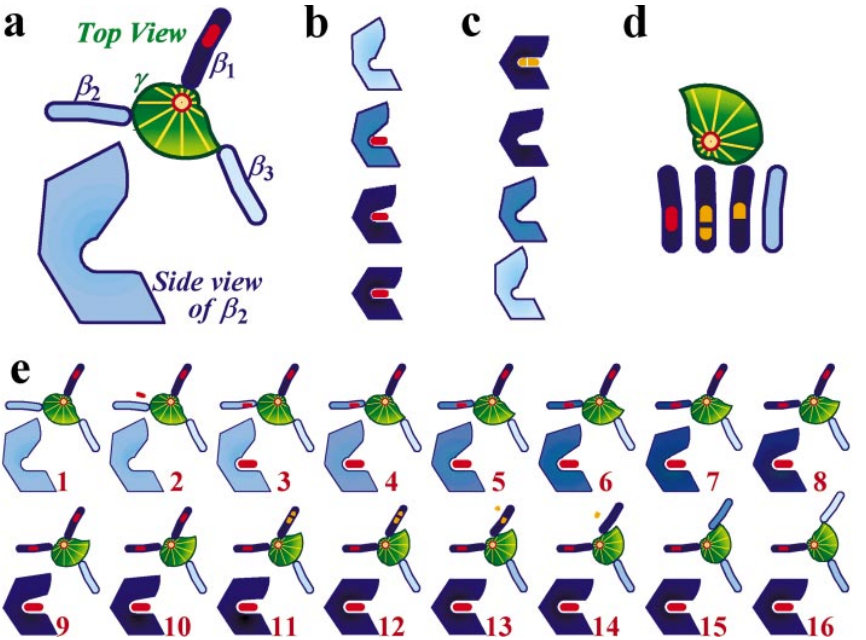

Figure 6 A camshaft model for the F_1 motor. Red oblong represents ATP, which is split into larger (ADP) and smaller (Pi) orange pieces. (*a*) The cam (γ) is supposed to stay in contact with the upper tip of βs, as if a thin oil layer exists at the interfaces. (*b*) The basic driving force comes from a push by a β binding ATP (β_2 in *e*1–*e*10), and (*c*) a pull by a β from which ADP and Pi leave (β_1 in *e*13–*e*16). The shade of blue reflects the degree of bending of β. (*d*) In addition, the upper tip of β is assumed to be twisted upon ATP hydrolysis, such that the tip motion produces a small amount of counterclockwise rotation (*e*10–*e*14). Conversely, a β with its tip twisted to the right (facing γ) has a higher affinity for ADP, whereas a tip twisted to the left favors ATP. (*e*) Sequence of events during hydrolysis. When γ is forced to rotate clockwise by an external torque (reversed sequence), the twist of the tip to the right in *e*16–*e*13 helps preferential binding of ADP over ATP.

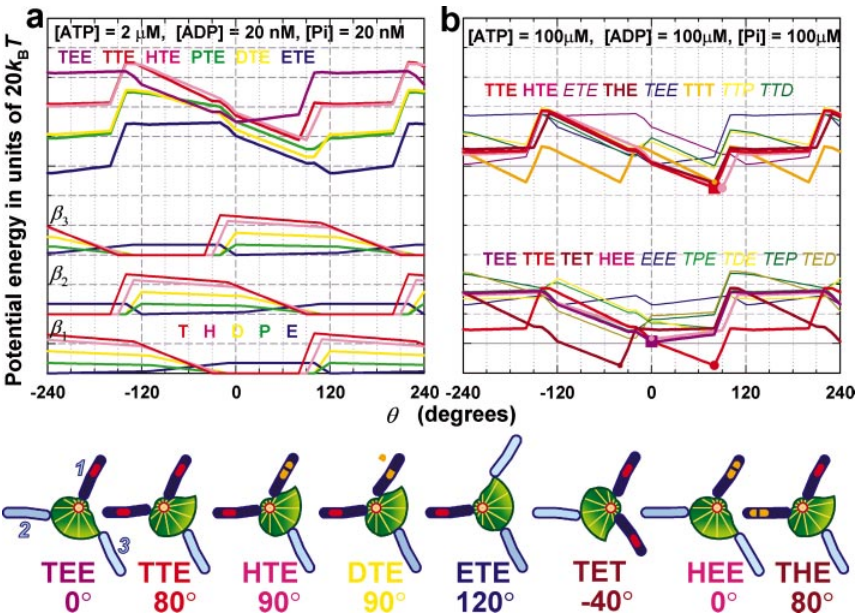

Figure 7 Potential energies for the camshaft model. T, ATP; H, hydrolysis products (ADP + Pi); D, ADP; P, Pi; E, empty. (*a*) Potential diagrams for the interaction between γ and an individual β (*bottom*), and the diagram for a major reaction pathway (*top*). (*b*) Diagrams showing all possible intermediates accessible from TEE (*bottom*) and TTE (*top*). Except for the three sets of curves at the bottom of (*a*), curves in a set are shifted vertically such that they represent angle-dependent free energy of the motor and environment, as explained in text.

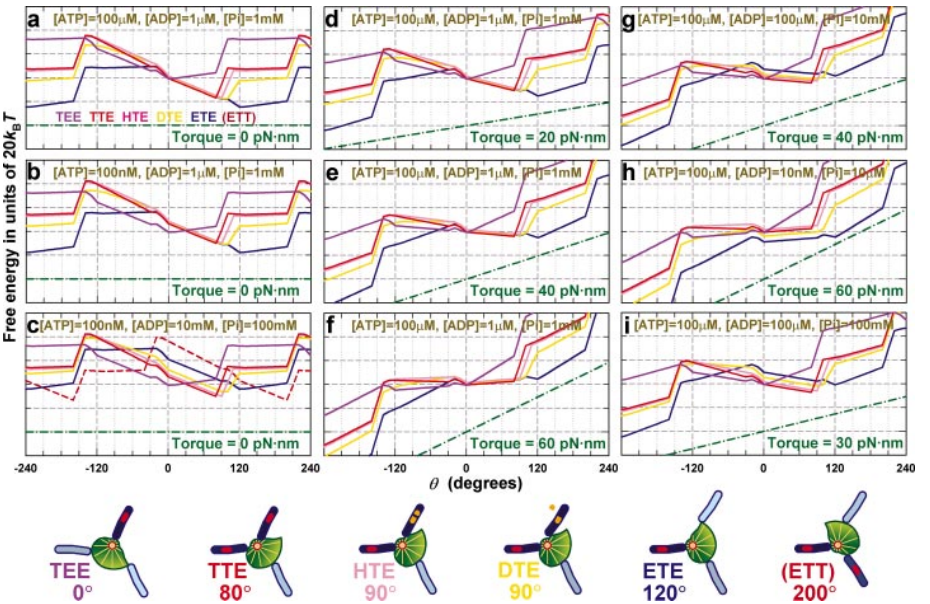

Figure 8 Potential diagrams under different ΔG and external torque. In (*a*)–(*i*), nucleotide concentrations are shown at the top and torque is shown at the bottom. The potential energy for the external torque is shown in a green line and has been added to all free-energy curves.

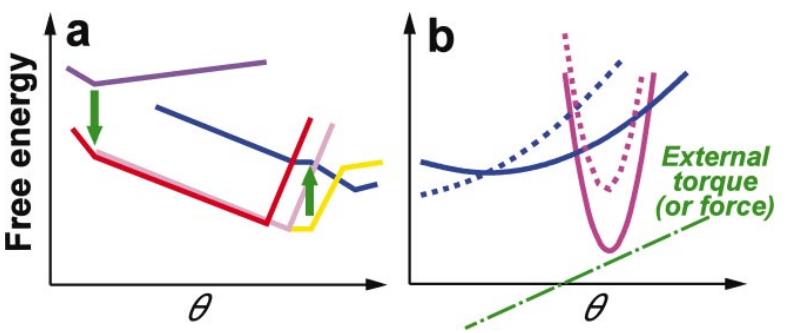

Figure 9 Designing a molecular machine. (*a*) A portion of free-energy diagram (around 0°–120°) for the camshaft model showing TEE (*purple*) to ETE (*blue*). ΔG is the same as in Figure 8*a*, but [ATP] (or K_{a0}^{ATP}) is higher and [ADP] (or K_{d0}^{ATP}) is lower. Thus, ATP binding is downhill (*downward arrow*), whereas ADP release is uphill (*upward arrow*). (*b*) Parabolic potential energies present a high barrier in the presence of an external torque (*dotted lines*).

Annual Review of Biophysics and Biomolecular Structure
Volume 33, 2004

CONTENTS